Active Dynamic Aggregation Model for Distributed Integrated Energy System as Virtual Power Plant

Haotian Zhao, Bin Wang, Xuanyuan Wang, Zhaoguang Pan, Hongbin Sun, Zhen Liu, and Qinglai Guo

***Abstract*—Distributed integrated multi-energy systems (DIMSs) can be regarded as virtual power plants to provide additional flexibility to the power system. This paper proposes a robust active dynamic aggregation model for the DIMSs to describe the maximum feasible region. The aggregation model includes the power constraints, energy constraints, and ramping constraints to aggregate different types of resources in the DIMSs. The proposed generator-like and storage-like model does not depend on the ancillary service market and can be directly incorporated into the economic dispatch model of the power system. A novel algorithm based on the column-and-constraint generation algorithm and convex-concave procedure is proposed to solve the two-stage robust optimization problem, which is more efficient than the KKT-based algorithms. Finally, a case study of an actual DIMS is developed to demonstrate the effectiveness of the proposed model.**

***Index Terms*—Aggregation, distributed integrated energy system (DIMS), robust optimization, virtual power plant.**

NOMENCLATURE

A. Sets and Parameters

Υ	Set of economic dispatch periods
Ω	Uncertainty set
ε_{CCP}	Convergence tolerance of the convex-concave procedure (CCP)
ε	Convergence tolerance of upper power value *UB*
$\eta^{EB,i}$	Efficiency of electric boiler i
$\eta^{c,i}, \eta^{dc,i}$	Charging and discharging efficiency of battery i
$c_t^{p,\min}$, $c_t^{p,\max}$	Weight coefficients of the lower and upper power bounds at period t
$c_t^{e,\min}$, $c_t^{e,\max}$	Weight coefficients of the lower and upper energy bounds at period t
c^{rd}, c^{ru}	Weight coefficient of the downward and upward ramping bounds
COP^i	Coefficient of performance (COP) of electric chiller i
EP^i	Set of the extreme points of the feasible operation region of combined heat and power (CHP) unit i
$E^{i,\max}, E^{i,\min}$	Maximum and minimum stored energy in battery i
$\boldsymbol{F}$	Feasible region of the recourse problem
$H_t^{L,i}$, $H_t^{CL,i}$, $P_t^{L,i}$	Predicted heating, cooling, and electric loads
l	Current iteration number
R	Initial value of the ramping bound of the aggregation model
$P^{\min}$, $P^{\max}$	Initial values of the lower and upper bound of the aggregation model
$P^{i,\max}, P^{i,\min}$	Maximum and minimum power outputs or consumptions of device i
$P_t^{i,pre}$	Predicted available power of renewable unit i
P_i^k, H_i^k	Electricity and heat productions corresponding to the k^{th} extreme point in the feasible operation region of CHP unit i
P_0^i	Fixed power consumption of electric boiler or electric chiller i
$P^{c,i,\max}$, $P^{dc,i,\max}$	Maximum charging and discharging power of battery i
$p_{t,*}^{VPP}$	Optimal solution of sub-problem
$\bar{p}_{t,*}^{k-1}$, $\underline{p}_{t,*}^{k-1}$, $\bar{e}_{t,*}^{k-1}$, $\underline{e}_{t,*}^{k-1}$, $r_*^{u,k-1}$, $r_*^{d,k-1}$	Optimal values of multi-energy virtual power plant (MEVPP) parameters solved by the master problem in the $(k-1)^{\text{th}}$ iteration
$R^{i,u}, R^{i,d}$	Upward and downward ramping rates of device i
S_{AC}, S_{GB}	Sets of absorption chillers and gas boilers

Manuscript received: March 31, 2020; accepted: August 19, 2020. Date of CrossCheck: August 19, 2020. Date of online publication: September 26, 2020.

This work was supported by the Science and Technology Project of State Grid Corporation of China (No. 52010119000Q).

H. Zhao, B. Wang, Z. Pan, H. Sun (corresponding author), and Q. Guo are with State Key Laboratory of Control and Simulation of Power System and Generation Equipments, Department of Electrical Engineering, Tsinghua University, Beijing, China (e-mail: zhao-ht17@mails.tsinghua.edu.cn; wb1984@tsinghua.edu.cn; panzg09@163.com; shb@tsinghua.edu.cn; guoqinglai@tsinghua.edu.cn).

X. Wang and Z. Liu are with the State Grid Jibei Electric Power Co., Ltd., Beijing, China (e-mail: wang.xuanyuan@jibei.sgcc.com.cn; liu.zhen.sgcc@outlook.com).

DOI: 10.35833/MPCE.2020.000202

S_{CHP}, S_G, S_W	Sets of CHP units, generators, and renewable units
S_{CL}, S_{HL}	Sets of cooling and heating loads
S_{EB}, S_{EC}	Sets of electric boilers and chillers
S_{ES}	Set of the batteries
s^i	Loss rate of battery i

B. Variables

δ_t^+, δ_t^-	Slack variables of energy balance constraint at period t
σ^i	Penalty factor restricting frequent start-up and shut-down of devices
$\lambda_t^{i,k}$	The k^{th} combination factor of CHP i
η	Auxiliary variable in C&CG algorithm
ω	Vector of dual variables
b_t^i	Binary decision variable that corresponds to the unit commitment status of device i at period t
$\underline{e}_t$, $\bar{e}_t$	Lower and upper energy bounds of aggregation model at period t
e_t^i	Energy stored in battery i at period t
h_t^i	Heat power output of CHP i at period t
p_t^{VPP}	Power consumed by virtual power plant (VPP) at period t
$p_{t,0}^{VPP}$, $\omega_{t,0}^E$	Current values of p_t^{VPP} and ω_t^E
$\underline{p}_t$, $\bar{p}_t$	Lower and upper power bounds of aggregation model at period t
p_t^i	Output power or consumed power of device i at period t
$p_t^{c,i}$, $p_t^{dc,i}$	Charging and discharging power of battery i at period t
r^d, r^u	Downward and upward ramping bounds of aggregation model
$\boldsymbol{u}^k$	The worst-case scenario identified by sub-problem in the k^{th} iteration
z_t^i	Start-up variable of the device i at period t
$z^{p,k}$, $z^{r,k}$, $z^{e,k}$	Auxiliary binary variables that determine which parameter in the aggregation model is modified in the k^{th} iteration

I. Introduction

THE purpose of the distributed integrated multi-energy system (DIMS) is to release more flexibility to enhance the security and reduce the operation cost of the energy system [1]-[3]. Additional flexibility is essential to reduce the renewable energy curtailment, for example, flexibility brought by the district heating system is beneficial to the wind power integration in Northern China [4], [5].

The coordination of multi energies exploits more flexibility. In [5], the pipeline energy storage of the heating network was considered to manage the variability of wind energy. In [6], the flexibility of the combined heat and power (CHP) system was improved by the coordination of different types of heat sources and large-scale heat storage tanks. In [7], the flexibility at the demand side was explored. The district heating systems considering the thermal inertia of the commercial buildings was aggregated and provided flexibility for the power system [8]. In [9], [10], an innovative theoretical framework was established for tailoring distributed control to practical implementations of microgrid clusters, providing a creative perspective on distributed energy management, and featuring significantly enhanced efficiency, flexibility, reliability, and resilience. A DIMS can be regarded as a multi-energy virtual power plant (MEVPP) to provide additional flexibility to the power system and gain profits simultaneously. This paper focuses on the aggregation method of the DIMS-based MEVPP.

Some previous related works proposed the aggregation model for the virtual power plant (VPP). Stochastic optimization [11] and two-stage robust optimization (RO)[12] models were presented for the offering strategy of a VPP in the energy and reserve market where the flexibility of the VPP is modeled as the reserve capacity. In [13], the aggregation of flexible loads effectively improved the power system flexibility. These studies aggregated the distributed resources according to the price in the wholesale market and the ancillary service market, acting as a "passive" VPP. However, the ancillary service market is not refined in many places. In this paper, we propose an "active" aggregation model for the DIMS-based MEVPP, which can interact with the power system directly without the ancillary service market.

An "active" aggregation model can be directly incorporated into the economic dispatch of the power system and it is independent of the ancillary service market. The generator-like and storage-like model is suitable for "active" aggregation. In [14], a generator-like model including output bounds, ramping rates, and cost functions was proposed to aggregate the energy-intensive enterprises, but storage devices and multi-energy conversion devices were not considered. In [15], the thermostatically controlled loads were aggregated as two types of the storage-like model. In [8], an aggregation model was formulated to describe the feasible region of the VPP, which consists of district heating loads considering thermal inertia. The greedy algorithm based on the sensitivity of linear programming problems was utilized to modify the feasible region. In this paper, we propose a standard dynamic aggregation model for active MEVPPs. The proposed model includes power generation constraints, ramping constraints, and energy constraints. This generator-like and storage-like model can be directly incorporated into the model of the power system. The ramping constraints and energy constraints are dynamic constraints, which represent the constraints on distributed generators and storage-like devices, respectively. The proposed model maximizes the feasible region of the DIMS, which provides maximum flexibility as a MEVPP to the power system.

Like [14], the proposed model is formulated as a two-stage RO problem. Dual norm [16], Benders decomposition [17], and column-and-constraint generation (C&CG) algorithm [18] are the most commonly used algorithms to solve the two-stage RO problem. The C&CG algorithm can achieve better performance in most cases [18], [19]. The sub-

problem of the C&CG algorithm is a bi-level max-min problem. In [14] and [19], Karush-Kuhn-Tucker (KKT) condition was utilized to transform the bi-level problem into a single-level problem. But the dynamic constraints in the model make it quite time-consuming. To improve the calculation efficiency, a novel algorithm based on a piecewise linearization (PWL) technique and convex-concave procedure (CCP) [20] is proposed in this paper to solve the sub-problem of the C&CG algorithm.

Main contributions of this paper are listed as follows.

1) A standard dynamic aggregation model is proposed for the DIMS-based MEVPP to aggregate multiple types of distributed resources. This generator-like and storage-like model can be directly incorporated into the model of the power system.

2) A two-stage RO model is proposed to acquire the optimal parameters of the proposed aggregation model, which maximizes the feasible region of the DIMS.

3) A novel algorithm based on the PWL technique and CCP is proposed to solve the sub-problem of the C&CG algorithm, which can greatly reduce the calculation time and derive a satisfactory solution.

The rest of this paper is organized as follows. Section II describes the proposed aggregation model. Section III develops the proposed algorithm to solve the two-stage RO problem. Results from a case study are analyzed in Section IV. Conclusions are drawn in Section V.

II. Robust Dynamic Aggregation Model

A. Model Description

In this paper, the interaction framework between the DIMS and the power system is described as follows.

1) The aggregation model and cost functions are calculated and sent to the power system. This paper focuses on this step.

2) The power system sends the dispatching signals to the DIMS.

3) The DIMS disaggregates the dispatching signals to the distributed resources.

Figure 1 shows the schematic diagram of the interaction.

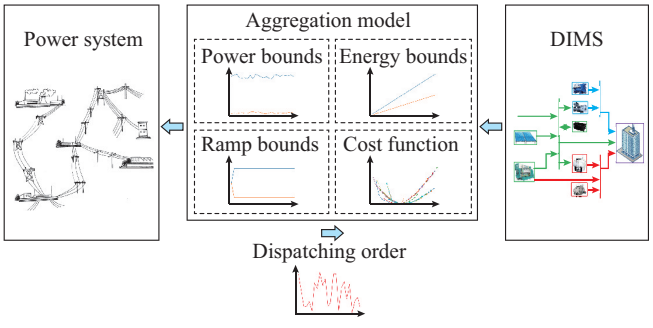

Fig. 1. Interaction between power system and DIMS.

The proposed model orients towards DIMS-based MEVPP of regional multi-energy systems, for example, the multi-energy industrial parks. The heating and cooling energy are balanced inside the DIMS and the electric power can be exchanged through the tie-line. Multiple types of energy conversion devices and energy storage devices are considered. The dynamic aggregated generator-like and storage-like model consists of constraints (1)-(3):

$$\underline{p}_t \le p_t^{VPP} \le \bar{p}_t \quad \forall t \in \Upsilon \tag{1}$$

$$\underline{e}_t \le \sum_{\tau=1}^{t} p_\tau^{VPP} \le \bar{e}_t \quad \forall t \in \Upsilon \tag{2}$$

$$-r^d \le p_t^{VPP} - p_{t-1}^{VPP} \le r^u \quad \forall t \in \Upsilon \setminus \{1\} \tag{3}$$

Formula (1) indicates the electric power generation (or charging/discharging) constraints; (2) indicates the energy constraints; and (3) indicates the ramping constraints.

For an active MEVPP participating in the day-ahead economic dispatching, the power violation between the MEVPP and the dispatching signals is restricted. Hence, we propose a robust aggregation model to guarantee that all dispatching signals which satisfy (1)-(3) can be realized by the DIMS. Constraints (2) and (3) can enlarge the feasible region. The robust feasible region of a MEVPP only composed of batteries is empty if the aggregation model only includes constraint (1). To incorporate various distributed resources in the MEVPP, dynamic constraints (2) and (3) are included in the aggregation model. The energy constraint (2) may be slack and inactive in the last periods. This constraint restricts the total energy from the first dispatching period. Constraint (2) can be replaced by the constraint which restricts the total energy in several adjacent dispatching periods, and the proposed algorithm is still valid.

The power bounds and energy bounds of the MEVPP are time-varying because the load profiles and the output of the renewable units are time-varying. The parameters in the ramping constraints are time-irrelevant because the ramping rate of the devices does not change over time.

The DIMS is limited in a relatively small geographical scale. Hence, the network constraints are omitted.

B. Cost Calculation

Different from the passive MEVPP, the active MEVPP sends cost information to the power system. We have proposed a heuristic method in [21] to calculate the PWL cost function of the MEVPP. The charging or discharging power of the batteries in the MEVPP is fixed according to the baseline. The economic dispatching results can be seen as the baseline, which is defined as the power of the tie line if there is no reserve deployment [22], [23]. At each calculation point, an one-time-slot economic dispatching optimization problem with slack variables in the electric energy balance constraint is solved. The values of the slack variables represent the adjustment of the batteries and a penalty term are added to the corresponding cost. In [21], the penalty factor is selected as the difference of the maximum and minimum time-of-use (TOU) electric prices, indicating the worst-case additional costs of the batteries.

If the ramping constraints are relaxed, the actual costs will be strictly less than that calculated by the cost functions. For DIMS, a majority of gas-fired distributed energy sources can ramp quickly, and the actual additional costs by the adjust-

ment of the charging plan of the batteries are usually less than the worst-case costs. Hence, this heuristic method is utilized in this paper to calculate the cost functions of the MEVPP. The actual additional costs of following the dispatching orders is ensured not to exceed that calculated by the cost functions in most cases.

The MEVPP can gain additional costs by bidding higher cost functions. The bidding strategy is beyond this paper.

C. Aggregation Model Formulation

The mathematical formulation of the aggregation model is a two-stage RO problem, where multi-energy distributed resources including generators, renewable units, CHP units, gas boilers (GBs), gas-fired absorption chillers (ACs), electric boilers (EBs), and electric chillers (ECs) are considered. The first-stage decision variables include the parameters of the aggregation model and the unit commitment variables. The output of the devices and the charging/discharging power of the storage devices are the second-stage decision variables:

$$\begin{cases} \min\limits_{\boldsymbol{y}} \sum\limits_{t\in\Upsilon}(c_t^{p,\min}\underline{p}_t - c_t^{p,\max}\bar{p}_t + c_t^{e,\min}\underline{e}_t - c_t^{e,\max}\bar{e}_t) - c^{ru}r^u - \\ \qquad c^{rd}r^d + \sum\limits_{t\in\Upsilon}\sum\limits_{i\in S_D}\sigma^i z_t^i + \max\limits_{p_t^{VPP}\in\Omega}\min\limits_{\boldsymbol{x}\in\boldsymbol{F}}\sum\limits_{t\in\Upsilon}M(\delta_t^+ + \delta_t^-) \\ S_D = S_G \cup S_{CHP} \cup S_{GB} \cup S_{AC} \cup S_{EB} \cup S_{EC} \end{cases} \tag{4}$$

where $\boldsymbol{y}$=[$\underline{p}_t$ $\bar{p}_t$ $\underline{e}_t$ $\bar{e}_t$ r^u r^d b_t^i z_t^i]; and $\boldsymbol{x}$=[p_t^i $\lambda_t^{i,k}$ $p_t^{c,i}$ $p_t^{dc,i}$ e_t^i].

The objective function (4) maximizes the feasible region of the aggregation model, where M is a large factor. The weight coefficients can affect the aggregation model. For example, a larger $c_t^{p,\max}$ leads to a larger $\bar{p}_t$, but relatively smaller energy upper bounds and ramping rates. The last term in the first-stage objective function is a penalty term restricting the frequent start-up and shut-down of the devices. The second-stage objective function is the total energy deviation of the MEVPP between the dispatching signals.

The constraints of the first-stage decision variables are as follows.

1) Constraints on parameters

$$\begin{cases} P^{\min} \le \underline{p}_t \le \bar{p}_t \le P^{\max} & \forall t\in\Upsilon \\ tP^{\min} \le \underline{e}_t \le \bar{e}_t \le tP^{\max} & \forall t\in\Upsilon \\ r^u \le R, r^d \le R \end{cases} \tag{5}$$

The preciser the initial bounds of the parameters $P^{\min}$, $P^{\max}$, R are, the faster convergence becomes.

2) Unit commitment status constraints

$$b_t^i - b_{t-1}^i \le z_t^i \quad \forall t\in\Upsilon, \forall i\in S_D \tag{6}$$

The dispatching signals p_t^{VPP} are uncertainty variables in the uncertainty set Ω described as equation (7):

$$\begin{aligned} \Omega = \{p_t^{VPP} | \underline{p}_t \le p_t^{VPP} \le \bar{p}_t, \forall t\in\Upsilon;\ \underline{e}_t \le \sum_{t=1}^{t} p_\tau^{VPP} \le \bar{e}_t, \forall t\in\Upsilon; \\ -r^d \le p_t^{VPP} - p_{t-1}^{VPP} \le r^u, \forall t\in\Upsilon\setminus\{1\}\} \end{aligned} \tag{7}$$

The constraints of the max-min recourse problem are as follows.

1) Bound and ramping constraints of devices

$$b_t^i P^{i,\min} \le p_t^i \le b_t^i P^{i,\max} \quad \forall t\in\Upsilon, \forall i\in S_D\setminus S_{CHP} \tag{8}$$

$$0 \le \lambda_t^{i,k} \le 1 \quad \forall k\in EP^i, \forall t\in\Upsilon, \forall i\in S_{CHP} \tag{9}$$

$$\sum_{k\in EP^i}\lambda_t^{i,k} = b_t^{CHP,i} \quad \forall t\in\Upsilon, \forall i\in S_{CHP} \tag{10}$$

$$p_t^i = \sum_{k\in EP^i}\lambda_t^{i,k}P_i^k, h_t^i = \sum_{k\in EP^i}\lambda_t^{i,k}H_i^k \quad \forall t\in\Upsilon, \forall i\in S_{CHP} \tag{11}$$

$$\begin{cases} p_t^i - p_{t-1}^i \le b_{t-1}^i R^{i,u} + (1-b_{t-1}^i)P^{i,\max} & \forall t\in\Upsilon, \forall i\in S_D \\ p_{t-1}^i - p_t^i \le b_t^i R^{i,d} + (1-b_t^i)P^{i,\max} & \forall t\in\Upsilon, \forall i\in S_D \end{cases} \tag{12}$$

Constraint (8) bounds the output power of the devices except CHPs; constraints (9)-(11) describe the operation region of CHPs with the convex combination of the vertex points of the polygonal feasible region [24]; and constraint (12) expresses the downward and upward ramping limits of the devices.

2) Constraints on renewable units

$$0 \le p_t^i \le P_t^{i,pre} \quad \forall t\in\Upsilon, \forall i\in S_R \tag{13}$$

3) Constraints on batteries

$$\begin{cases} 0 \le p_t^{c,i} \le P^{c,i,\max} & \forall t\in\Upsilon, \forall i\in S_{ES} \\ 0 \le p_t^{dc,i} \le P^{dc,i,\max} & \forall t\in\Upsilon, \forall i\in S_{ES} \end{cases} \tag{14}$$

$$E^{i,\min} \le e_t^i \le E^{i,\max} \quad \forall t\in\Upsilon, \forall i\in S_{ES} \tag{15}$$

$$\begin{cases} e_1^i = E_0^i + \eta^{c,i}p_1^{c,i} - \dfrac{p_1^{dc,i}}{\eta^{dc,i}} & \forall i\in S_{ES} \\ e_t^i = (1-s^i)e_t^{i-1} + \eta^{c,i}p_t^{c,i} - \dfrac{p_t^{dc,i}}{\eta^{dc,i}} & \forall t\in\Upsilon\setminus\{1\}, \forall i\in S_{ES} \end{cases} \tag{16}$$

Constraint (14) defines the maximum charging and discharging power; constraint (15) restricts the energy stored in the battery; constraint (16) denotes the relationship between the energy stored and the exchanged power.

4) Energy balance constraints

$$\begin{aligned} p_t^{VPP} + \sum_{i\in S_G\cup S_R} p_t^i + \sum_{i\in S_{CHP}} p_t^i + \delta_t^+ + \delta_t^- = \sum_{i\in S_L} P_t^{L,i} + \\ \sum_{i\in S_{ES}}(p_t^{dc,i} - p_t^{c,i}) + \sum_{i\in S_{EB}\cup S_{EC}} p_t^i \quad \forall t\in\Upsilon \end{aligned} \tag{17}$$

$$\sum_{i\in S_{CHP}} h_t^i + \sum_{i\in S_{GB}} p_t^i + \sum_{i\in S_{EB}} \eta^{EB,i}p_t^i = \sum_{i\in S_{HL}} H_t^L \quad \forall t\in\Upsilon \tag{18}$$

$$\sum_{i\in S_{AC}} p_t^i + \sum_{i\in S_{EC}} COP^i \cdot p_t^i = \sum_{i\in S_{CL}} H_t^{CL} \quad \forall t\in\Upsilon \tag{19}$$

Constraints (17)-(19) enforce the energy balance between the generation supply and demand of electric, heat, and cooling, respectively.

For the sake of simplicity, the proposed two-stage RO formulation is rewritten in the matrix form as (20). The matrices $\boldsymbol{A}$, $\boldsymbol{H}$, $\boldsymbol{R}$, $\boldsymbol{E}$, $\boldsymbol{G}$, $\boldsymbol{J}$ and vectors $\boldsymbol{c}$, $\boldsymbol{d}$, $\boldsymbol{u}$, $\boldsymbol{q}$, $\boldsymbol{p}$ in (20) can be obtained from (4)-(19). Note that the uncertainty set is restricted by the first-stage decision variables.

$$\begin{cases} \min\limits_{\boldsymbol{y}} \boldsymbol{c}^{\mathrm{T}}\boldsymbol{y} + \max\limits_{\boldsymbol{u}\in\Omega}\min\limits_{\boldsymbol{x}\in\boldsymbol{F}} \boldsymbol{d}^{\mathrm{T}}\boldsymbol{x} \\ \text{s.t. } \boldsymbol{A}\boldsymbol{y} \ge \boldsymbol{b}, \boldsymbol{y} \ge \boldsymbol{0} \\ \quad \Omega = \{\boldsymbol{u} | \boldsymbol{H}\boldsymbol{u} + \boldsymbol{R}\boldsymbol{y} \ge \boldsymbol{q}\} \\ \quad \boldsymbol{F} = \{\boldsymbol{x} | \boldsymbol{x} \ge \boldsymbol{0}, \boldsymbol{E}\boldsymbol{y} + \boldsymbol{G}\boldsymbol{x} + \boldsymbol{J}\boldsymbol{u} \ge \boldsymbol{p}\} \end{cases} \tag{20}$$

III. Solution Methodology

In this paper, a master sub-problem framework based on the C&CG algorithm is utilized to solve the two-stage RO problem. Different from the original C&CG algorithm [18], the solution methodology in this paper has two key points. Firstly, the column constraints added to the master problem are modified in the form of per-unit value. Compared with the branch-and-bound algorithm in [14], the proposed model utilizes a linearization method to solve the master problem. Secondly, this paper proposes a novel algorithm based on PWL technique and CCP to solve the sub-problem more efficiently compared with the KKT-based algorithms in [14] or [19]. The details are as follows.

A. Master Problem

The master problem calculates the optimal parameters of the aggregation model and decides the commitment status of the devices against all the scenarios identified by the sub-problem:

$$\begin{cases} \min\limits_{\boldsymbol{y}} \boldsymbol{cy}+\eta \\ \text{s.t. } \boldsymbol{Ay}\ge\boldsymbol{b} \quad \boldsymbol{y}\ge 0 \\ \quad \eta\ge \boldsymbol{d}^{\mathrm{T}}\boldsymbol{x}^{k} \quad k=1,2,...,l \\ \quad \boldsymbol{Ey}+\boldsymbol{Gx}^{k}+\boldsymbol{Ju}^{k}\ge\boldsymbol{p} \quad \boldsymbol{x}^{k}\ge 0, k=1,2,...,l \end{cases} \tag{21}$$

In the proposed two-stage RO model, the uncertainty set is correlated to the value of the first-stage decision variables. Hence, the uncertainty in the column constraints added to the master problem is expressed in per-unit value:

$$\begin{cases} u_t^k = z^{p,k}p_t^* + z^{r,k}\left(p_1^* + \sum\limits_{\tau=2}^{t} r_\tau^*\right) + z^{e,k}(e_t^* - e_{t-1}^*) \\ \boldsymbol{u}^k = [u_1^k \quad u_2^k \quad ... \quad u_T^k]^{\mathrm{T}} \\ z^{p,k}+z^{e,k}+z^{r,k}=1 \end{cases} \tag{22}$$

The auxiliary variables $z^{p,k}$, $z^{r,k}$ and $z^{e,k}$ determine which parameter in the aggregation model is modified. For example, $z^{p,k}=1$ indicates that the power bounds of the MEVPP, i.e., $\bar{p}_t$ and $\underline{p}_t$ in (1) are modified in the k^{th} iteration based on the impact of the added constraint. p_t^*, e_t^* and r_t^* are in the form of (23)-(25):

$$p_t^* = \frac{p_{t,*}^{VPP} - \underline{p}_{t,*}^{k-1}}{\bar{p}_{t,*}^{k-1} - \underline{p}_{t,*}^{k-1}}(\bar{p}_t - \underline{p}_t) + \underline{p}_t \tag{23}$$

$$e_t^* = \frac{\sum\limits_{\tau=1}^{t} p_{\tau,*}^{VPP} - \underline{e}_{t,*}^{k-1}}{\bar{e}_{t,*}^{k-1} - \underline{e}_{t,*}^{k-1}}(\bar{e}_t - \underline{e}_t) + \underline{e}_t \tag{24}$$

$$r_t^* = \begin{cases} \dfrac{p_{t,*}^{VPP} - p_{t-1,*}^{VPP}}{r_*^{u,k-1}} r^u & p_{t,*}^{VPP} - p_{t-1,*}^{VPP} \ge 0 \\ \dfrac{p_{t,*}^{VPP} - p_{t-1,*}^{VPP}}{r_*^{d,k-1}} r^d & p_{t,*}^{VPP} - p_{t-1,*}^{VPP} < 0 \end{cases} \tag{25}$$

All the constraints in the master problem are linear except (22). The products of a binary variable and a continuous variable in (22) are linearized by the big-M method [12]. After linearization, the master problem is a mixed-integer linear programming (MILP) problem, which can be solved by the off-the-shelf software.

B. Sub-problem

The sub-problem is a bi-level max-min problem identifying the worst-case scenario with the fixed first-stage decision variables $\boldsymbol{y}^*$ calculated in the master problem:

$$\begin{cases} \max\limits_{\boldsymbol{u}\in\Omega} \min\limits_{\boldsymbol{x}\in\boldsymbol{F}} \boldsymbol{d}^{\mathrm{T}}\boldsymbol{x} \\ \text{s.t. } \boldsymbol{Hu}+\boldsymbol{Ry}^*\ge\boldsymbol{q} \\ \quad \boldsymbol{Ey}^*+\boldsymbol{Gx}+\boldsymbol{Ju}\ge\boldsymbol{p} \end{cases} \tag{26}$$

Transforming (26) into a single-level optimization with KKT condition is the most common method to solve the max-min problem [14], [18], [19]. However, the complementary constraints brought by the KKT condition make the problem time-consuming to solve. The time-coupled constraints (2) and (3) greatly increase the solution time. Hence, duality theorem rather than KKT condition is utilized for the transformation:

$$\begin{cases} \max\limits_{\boldsymbol{u},\boldsymbol{\omega}} \boldsymbol{\omega} \\ \text{s.t. } \boldsymbol{G}^{\mathrm{T}}\boldsymbol{\omega}\le\boldsymbol{d} \\ \quad \boldsymbol{Hu}+\boldsymbol{Ry}^*\ge\boldsymbol{q} \\ \quad \boldsymbol{\omega}\ge\boldsymbol{0} \end{cases} \tag{27}$$

Fomula (27) is a bilinear programming (BP) problem. BP is hard to be solved globally because of nonconvexity. Some commercial software, such as the newly released Gurobi 9.0.0 [25], can solve the BP globally, but it takes a long time. A novel solution algorithm based on CCP is proposed in this paper, which is more efficient to solve this problem and the error is acceptable.

The objective function in (27) is reformulated as:

$$\max_{\boldsymbol{u},\boldsymbol{\omega}} (\boldsymbol{p}-\boldsymbol{Ey}^*)^{\mathrm{T}}\boldsymbol{\omega} - \sum_{t\in\Upsilon} p_t^{VPP}\omega_t^E \tag{28}$$

where ω_t^E is the dual variable of constraint (17). The bilinear terms in (28) are reformulated as the difference of quadratic terms:

$$\max_{\boldsymbol{u},\boldsymbol{\omega}} \boldsymbol{\omega} - \frac{1}{2}\sum_{t\in\Upsilon}(p_t^{VPP}+\omega_t^E)^2 + \frac{1}{2}\sum_{t\in\Upsilon}(p_t^{VPP})^2 + \frac{1}{2}\sum_{t\in\Upsilon}(\omega_t^E)^2 \tag{29}$$

In (29), the first two terms are concave in the maximization problem and the last two terms are convex. Hence, (29) is in the form of difference of convex functions. CCP is used to heuristically solve the problem. The CCP algorithm is highly dependent on the initial point [20], hence, we have proposed a linearization method to provide a suitable initial value for the CCP. Besides, the bilinear terms in the objective function are reformulated as the difference of convex terms, and the negative convex term in the maximization problem can be linearized without additional integer variables. This linearization method can efficiently provide a suitable initial value in several seconds.

The incremental formulation for the PWL is applied to the quadratic terms in (29), which has shown the best performance in nonconvex quadratic programming problems, such as the gas network optimization problems [26]. In the PWL formulation, continuous auxiliary variables π_i and binary auxiliary variables ψ_i are introduced. Each quadratic term χ^2 is linearized as (30)-(33):

$$\chi=\chi_1+\sum_{i=1}^{N}(\chi_{i+1}-\chi_i)\pi_i \tag{30}$$

$$\chi^2\approx\chi_1^2+\sum_{i=1}^{N}(\chi_{i+1}^2-\chi_i^2)\pi_i \tag{31}$$

$$0\le\pi_i\le 1 \quad i=1,2,...,N \tag{32}$$

$$\pi_{i+1}\le\psi_i\le\pi_i \quad \psi_i\in\{0,1\},i=1,2,...,N-1 \tag{33}$$

The negative quadratic term is concave in the maximization problem, hence constraint (33) and the binary auxiliary variables ψ_i corresponding to the negative quadratic term in (29) can be eliminated to increase computation speed. We can select a larger N for the negative quadratic terms but a smaller N for the positive quadratic terms for better performance. The sub-problem (27) is linearized to a MILP and initializes the CCP algorithm. In addition, dual variables ω_t^E are bounded with range $[-M,M]$ symmetrical about 0. Hence, we select N for $(\omega_t^E)^2$ as even numbers.

The CCP algorithm solves a sequence of quadratic programming (QP) problems as (34):

$$\begin{cases}\max\limits_{\boldsymbol{u},\boldsymbol{\omega}}\ \boldsymbol{\omega}-\dfrac{1}{2}\sum\limits_{t\in\Upsilon}(f(p_t^{VPP},\omega_t^E)-\tilde{g}(p_t^{VPP},\omega_t^E))\\ \text{s.t.}\ \ \boldsymbol{G}^{\mathrm{T}}\boldsymbol{\omega}\le\boldsymbol{d}\\ \qquad \boldsymbol{Hu}+\boldsymbol{Ry}^*\ge\boldsymbol{q}\\ \qquad \boldsymbol{\omega}\ge\boldsymbol{0}\end{cases} \tag{34}$$

$$\begin{cases}f(p_t^{VPP},\omega_t^E)=(p_t^{VPP}+\omega_t^E)^2\\ \tilde{g}(p_t^{VPP},\omega_t^E)=(p_{t,0}^{VPP})^2+(\omega_{t,0}^E)^2+2\omega_{t,0}^E(\omega_t^E-\omega_{t,0}^E)+\\ \qquad\qquad 2p_{t,0}^{VPP}(p_t^{VPP}-p_{t,0}^{VPP})\end{cases} \tag{35}$$

Update the convex approximation $\tilde{g}(p_t^{VPP},\omega_t^E)$ and solve (34) iteratively until the stop creation of CCP is satisfied to derive the heuristic optimal solution of the sub-problem. Then, add the column constraints (36) to the master problem.

$$\begin{cases}\eta\ge\boldsymbol{d}^{\mathrm{T}}\boldsymbol{x}^k & k=1,2,...,l\\ \mathbf{Ey}+\mathbf{Gx}^k+\mathbf{Ju}^k\ge\boldsymbol{p} & \boldsymbol{x}^k\ge 0,k=1,2,...,l\end{cases} \tag{36}$$

C. Summarization of Algorithm

In summary, the proposed two-stage RO model (20) is solved by the following steps.

Step 1: initialize the bounds of the parameters of the aggregation model in (5). Set the upper bound value UB = 0, and set the iteration number l=0.

Step 2: solve the master problem (21) and derive the optimal solution y^*.

Step 3: solve the linearized sub-problem with fixed y^* to derive an initial point for CCP. Set the iteration number m=0.

Step 4: solve the convexified QP (34) and derive the optimal solution $p_{t,m}^{VPP}$, $\omega_{t,m}^E$ and the optimal value of the objective function θ_m.

Step 5: if m=0 or $\left|\theta_m-\theta_{m-1}\right|>\varepsilon_{CCP}$, let $p_{t,0}^{VPP}=p_{t,m}^{VPP},\omega_{t,0}^E=\omega_{t,m}^E$ and convexify the problem according to (35), let $m=m+1$ and go to *Step 4*. Otherwise, let $p_{t,*}^{VPP}=p_{t,m}^{VPP}$ and go to *Step 6*.

Step 6: update $UB=\max\{UB,\theta_m\}$. If $UB\le\varepsilon$, where return $\boldsymbol{y}^*$ and terminate. Otherwise, calculate the column constraints according to (22)-(25). Create new variables $\boldsymbol{x}^k$ and add column constraints to the master problem according to (36), let $l=l+1$ and go to *Step 2*.

The flow chart of the proposed algorithm is shown in Fig. 2.

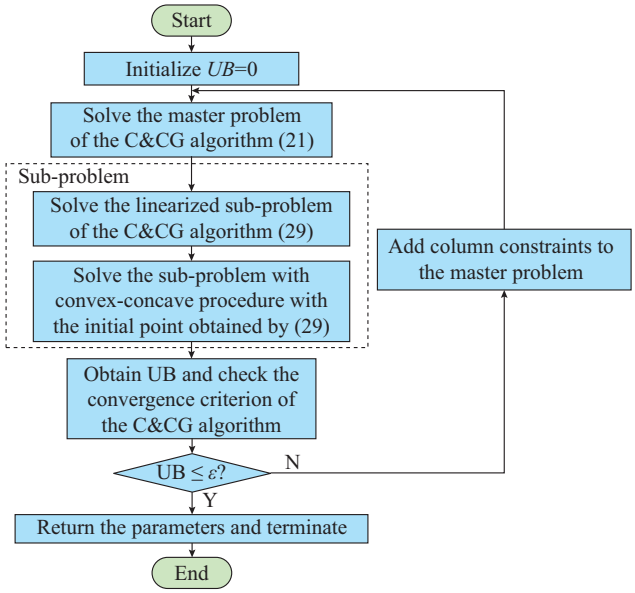

Fig. 2. Flow chart of proposed algorithm.

IV. Case Studies

In this section, case studies are conducted to test the performance of the proposed model and algorithm. The tests are performed on an HP laptop with an Intel i7-8750H CPU running at 2.20 GHz with 16 GB of memory. The proposed model is solved by Gurobi 9.0.0 [25] with C++ API coded in Visual Studio 2017 Community.

A. System Configuration

The test system is based on an industrial park located in Beijing, China. The enterprises in the industrial park require electricity, heating and cooling energy simultaneously. Heat and cooling energies are balanced inside the park. The industrial park is a typical DIMS, which consists of a diesel generator, a CHP unit, a photovoltaic (PV) cell, a GB, an EB, an AC, an EC, and a battery. Figure 3 shows the configuration of the test distributed integrated energy system. The energy consumed by the industrial park is defined as the positive direction of the power of the aggregation model. The industrial park uses heat for manufacture whereas cooling for commercial buildings, so the heating and cooling load profiles are similar to the electric load profile.

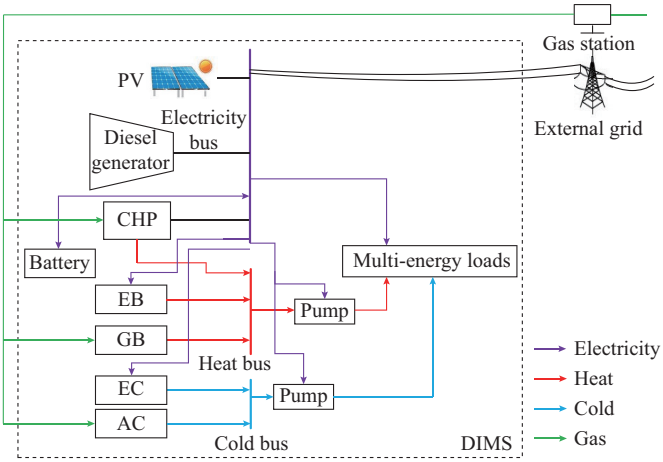

Fig. 3. Configuration of test DIMS.

The parameters of the test system are specified in [27]. The multi-energy load profiles are shown in Fig. 4. In this industrial park, the total electric load is larger than the installed generation capacity. Hence, the industrial park purchases power from the external grid. The weight factors are selected as Table I. The convergence tolerance ε is set to be 10^{-6}. The number of segments of the convex quadratic terms and nonconvex quadratic terms are selected as 5 and 2.

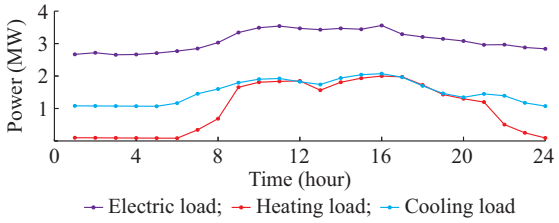

Fig. 4. Multi-energy load profiles.

TABLE I
PARAMETERS OF WEIGHT COEFFICIENTS

Weight factor	Value
$c_t^{p,\min}$, $c_t^{p,\max}$	15, 15
$c_t^{e,\min}$, $c_t^{e,\max}$	1, 1
c^{ru}, c^{rd}	0.2, 0.3

B. Simulation and Results

The simulation results are shown in Fig. 5, where the initial values of the aggregation parameters are in red lines and the final values are in blue lines. In the aggregation model, the trend of the upper power bound is similar to that of electric load. In addition, the heat and cooling power consumed by the multi-energy load can affect the upper power bound of the DIMS through the EB and the EC. The upper power bound is relatively higher at 08:00-16:00. The lower power bound almost remains unchanged over time because the fluctuation of the load profile can be offset by the PV cell. The upward and downward ramping rate of the aggregation model is 1.681 MW/h and 1.909 MW/h, respectively. The cost functions are shown in Fig. 6.

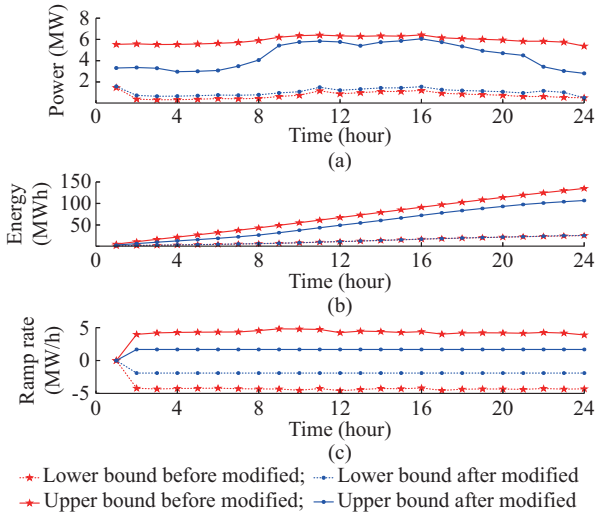

Fig. 5. Aggregation model of DIMS. (a) Power bounds. (b) Energy bounds. (c) Ramp bounds.

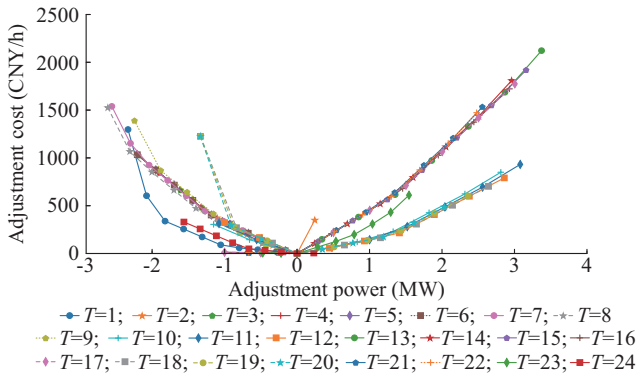

Fig. 6. Cost functions of DIMS.

Figure 7 shows the additional flexibility brought by the coordination of the multi-energy flows inside the DIMS. The red lines indicate the power bounds, energy bounds, and ramping bounds when multi-energy conversion devices are operated according to the results of optimal day-ahead economic dispatching, which means only electric resources including distributed generators and batteries can adjust their operation according to the dispatching signals. Hence, the CHP, the GB, the EB, the AC, and the EC do not provide flexibility to the power system and operate as the baseline. In contrast, the blue lines represent the aggregation models with the coordination of multi-energy conversion devices, for example, the EB and the EC can be shut down when the power system deploys downward reserve requests. The heat and cooling energy are provided by the gas-fired devices when the EB and the EC are shut down. Hence, flexibility brought by the coordination of multi-energy conversion devices is exploited and the energy balance constraints (18) and (19) still hold. In addition, the coordination of multi-energy conversion devices decouples the electric and heat output of the CHP. The CHP can provide more downward reserve capacities to the power system. Similarly, the coordination of multi-energy flow, especially the quick ramping capability of the electric-driven devices, provides higher ramping rates.

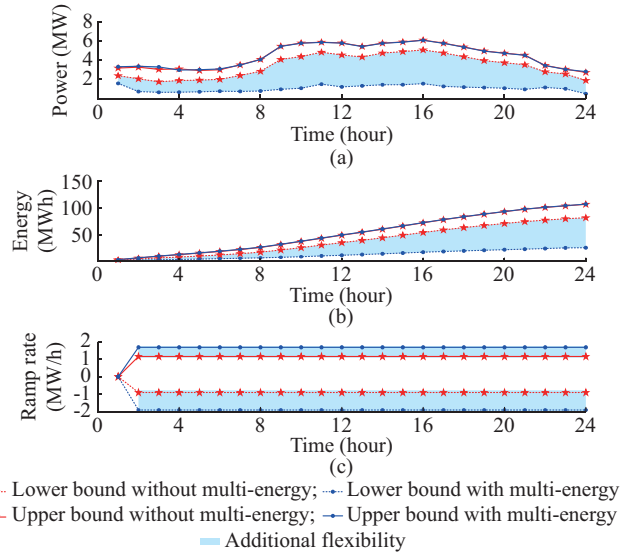

Fig. 7. Additional flexibility brought by coordination of multi-energy flows inside DIMS. (a) Power bounds. (b) Energy bounds. (c) Ramp bounds.

The dynamic constraints (2) and (3) in the aggregation model can fully reflect the actual feasible region of the DIMS. The robust power bounds with and without dynamic constraints are shown in Fig. 8. If dynamic constraints are excluded, the power bounds become tighter and the flexibility of the DIMS is not fully characterized. In this test case, if we ignore the dynamic constraints but regard the blue line in Fig. 8 as the power bounds, the maximum total violation is 7.2 MWh. The relative error is about 15% between the dispatching signals.

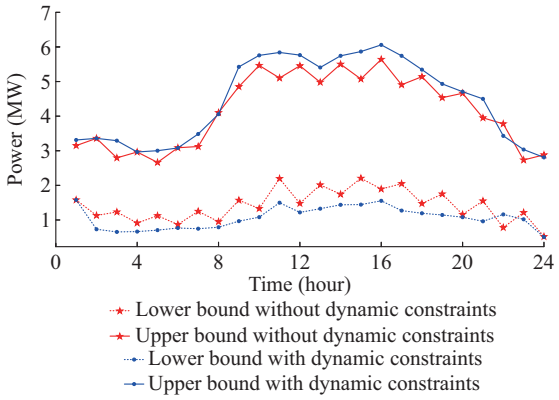

Fig. 8. Power bounds of aggregation model with and without dynamic constraints.

The parameters of the weight coefficients in (4) can affect the aggregation model. We set $c_t^{p,\min}$ to be 100 at 10:00-12:00, which suggests that the power system requires more downward reserve at the peak of the total load profile. The other weight coefficients remain unchanged as Table I. The aggregation results are shown in Fig. 9. The DIMS provides more downward flexibility at 10:00-12:00 by adjusting the charging plan of the battery. The battery is forced to be charged at 07:00-09:00. Hence, the stored energy in the battery can provide 0.33 MW additional downward reserve to the power system.

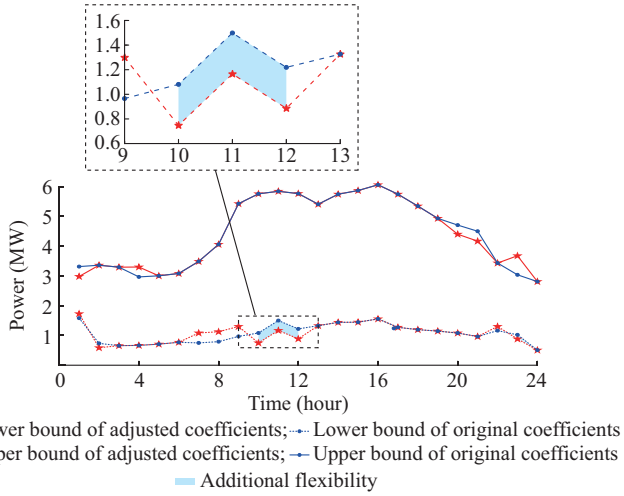

Fig. 9. Power bounds affected by values of coefficients.

The parameters of the weight coefficients in the aggregation model can be adjusted to meet the requirement of the power system. For example, the Jibei Power Grid in Northern China requires an upward reserve to reduce wind curtailment [28]. The parameters $c_t^{p,\max}$ and $c_t^{e,\max}$ can be set larger in the required dispatching periods.

The GB in the DIMS is a backup for heating. The installation of the GB can reduce the operation cost when TOU price is high and provide more flexibility. We have conducted a case study to compare the power bounds of the MEVPP with and without the GB.

As shown in Fig. 10, the MEVPP with a GB has lower power bounds at 09:00-20:00 because the EB is forced to open at that period to provide heat energy. When the MEVPP is equipped with a GB, the CHP and the EB can adjust their operation plans to realize the dispatching signals from the power system. Although the GB does not produce electric energy, it can provide about 0.6 MW downward reserve capacity when the heating load is larger than the capacity of the EB.

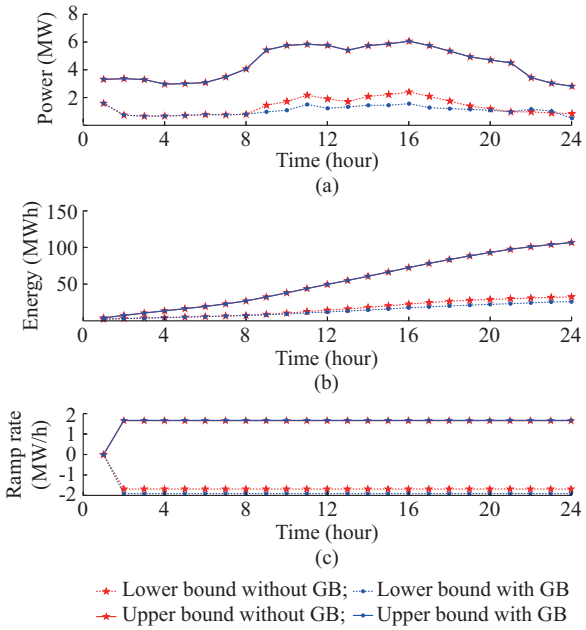

Fig. 10. Aggregation model with and without GB. (a) Power bounds. (b) Energy bounds. (c) Ramp bounds.

C. Calculation Efficiency

In this subsection, we compare the calculation efficiency with the KKT-based algorithm [14] and the Gurobi 9.0.0 nonconvex solver [25]. The algorithm in [14] utilized KKT conditions to transform the sub-problem into a single problem, with *Nc* additional complementary slackness constraints. *Nc* is the number of constraints (8)-(19) in the sub-problem. In [19], the sub-problem was transformed into (27) and the KKT condition was utilized to separate the bilinear terms in the objective function, with *Nu* additional complementary slackness constraints. *Nu* is the number of constraints (1)-(3) in the uncertainty set. *Nc* equals to 491 in the test system and *Nu* equals to 142. Hence, we utilize the MILP formulation in [19] to test the efficiency of the KKT-based algorithm. The time limit for a sub-problem in each iteration is set to 3600 s.

In Table II, the problem is successfully solved by the pro-

posed algorithm in 512 s, 72.26 s of which is for solving the PWL form of the sub-problem, 108.73 s is for CCP algorithm calculation, 86.59 s is for solving the master problem and 244 s is for IO and model extraction. The total iteration number of the C&CG algorithm is 20. The KKT-based algorithm and the Gurobi nonconvex solver fail to solve the problem in the time limit. The KKT-based algorithm takes about 1 hour to solve the sub-problem in the first iteration and it exceeds the time limit. The Gurobi nonconvex solver can solve the first several sub-problem in 1 min but it fails to solve the sub-problem in the 4th iteration in 1 hour.

TABLE II
CALCULATION EFFICIENCY OF DIFFERENT ALGORITHMS

No. of iterations	Time consumed by different algorithms (s)				
	The proposed algorithm			KKT-based algorithm	Gurobi nonconvex solver
	PWL	CCP	Total		
1st iteration	0.35	0.21	0.56	3535.66	2.05
2nd iteration	2.54	0.73	3.27	1939.09	37.57
3rd iteration	6.44	0.53	6.97	831.67	30.39
4th iteration	5.80	3.44	9.24	>3600	>3600
⋮	⋮	⋮	⋮	⋮	⋮
Total solution time	512.00			>3600	>3600

The objective values of the last iteration of the sub-problem with different segments are shown in Table III, which indicates the proposed algorithm is satisfactory in calculation accuracy. The number of segments of the convex quadratic terms and nonconvex quadratic terms are selected as 5 and 2, respectively. The objective value of the sub-problem is 2×10^{-11} and the algorithm terminates. If we increase the number of the segments, the objective value of the sub-problem increases and the worst-case scenario is added to the master problem to continue the iteration procedure. The selection of the number of the segments in Section III-B brings a maximum total deviation, 0.289 MWh, between the worst-case dispatching signals. The maximum relative deviation is 0.66%, which is acceptable in the day-ahead economic dispatching. Hence, the proposed algorithm is satisfactory in both precision and calculation speed.

TABLE III
OBJECTIVE VALUES OF SUB-PROBLEM IN LAST ITERATION

Segments of the convex term	Segments of the nonconvex term	Solution time (s)	Objective value
5	2	5.56	2.0000×10^{-11}
5	4	102.42	2.4087×10^{-1}
10	2	14.52	2.8905×10^{-1}
10000	2	9032.00	2.8905×10^{-1}
Gurobi (failed to converge in 20000 s)		-	2.8905×10^{-1}*

Note: * represents the lower bound of the objective function when the solver terminates.

D. Monte Carlo Simulation

In this subsection, the Monte Carlo simulation is conducted to test the feasibility of the proposed aggregation model. The optimal solution of the sub-problem corresponds to a vertex of the polyhedron uncertainty set, hence we generate 5000 samples on the vertexes of the aggregation model (1)-(3) to test the feasibility of the proposed model. The simulation results are shown in Fig. 11, where each sample is represented as a point.

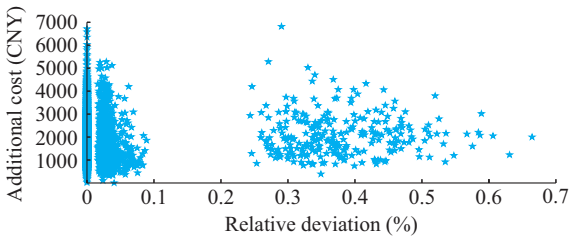

Fig. 11. Monte Carlo simulation.

The maximum total deviation is 0.289 MWh, which is the same as the result calculated in Section IV-C. The maximum relative total deviation from the dispatching order is 0.66% and the mean relative deviation is 0.028%. And 3386 samples of the dispatching signals can be realized by the DIMS without deviation. In addition, all calculated costs are higher than the actual costs, and the average difference between the calculated costs and the actual costs is 1798 CNY, about 3% of the total operation costs of the DIMS.

V. CONCLUSION

In this paper, the aggregation model of a DIMS-based MEVPP is studied. Based on the two-stage RO, the feasible region of the DIMS is described by the power constraints, energy constraints, and ramping constraints, which can be directly incorporated into the economic dispatching model of the power system. The proposed robust aggregation model can guarantee that all dispatching signals which satisfy the three constraints can be realized by the DIMS. The two-stage RO problem is solved based on the C&CG algorithm. The dynamic constraints, including the energy constraints and ramping constraints, make the sub-problem of the C&CG algorithm time-consuming to be solved. A novel algorithm based on CCP is proposed and a PWL method based on the convexity of the objective function is proposed to find an initial point for the CCP. The proposed algorithm can solve the bilinear sub-problem on a polygon set efficiently and is satisfactory in terms of accuracy. In case studies, the aggregation of a real DIMS in Beijing could adjust its power consumption in about 2-5 MW, which provides flexibility to the power system. The maximum power deviation is lower than 0.66%, which is in an acceptable range for day-ahead economic dispatching.

REFERENCES

[1] P. Mancarella, "MES (multi-energy systems): an overview of concepts and evaluation models," *Energy*, vol. 65, pp. 1-17, Feb. 2014.
[2] Y. Li, H. Zhang, X. Liang *et al.*, "Event-triggered-based distributed cooperative energy management for multienergy systems," *IEEE Transactions on Industrial Informatics*, vol. 15, no. 4, pp. 2008-2022, Apr. 2019.
[3] H. Zhang, Y. Li, D. Gao *et al.*, "Distributed optimal energy management for energy internet," *IEEE Transactions on Industrial Informatics*, vol. 13, no. 6, pp. 3081-3097, Dec. 2017.

[4] J. Li, F. Cai, L. Qiao *et al*. (2020, Jan.). 2014 China wind power review and outlook. [Online]. Available: http://www. indiaenvironmentportal. org. in/files/file/2014%20China% 20Wind% 20Power% 20Review. pdf
[5] Z. Li, W. Wu, M. Shahidehpour *et al*., "Combined heat and power dispatch considering pipeline energy storage of district heating network," *IEEE Transactions on Sustainable Energy*, vol. 7, no. 1, pp. 12-22, Jan. 2016.
[6] X. Chen, C. Kang, M. O'Malley *et al*., "Increasing the flexibility of combined heat and power for wind power integration in China: modeling and implications," *IEEE Transactions on Power Systems*, vol. 30, no. 4, pp. 1848-1857, Jul. 2015.
[7] L. Brange, J. Englund, and P. Lauenbur, "Prosumers in district heating networks—a Swedish case study," *Applied Energy*, vol. 164, pp. 492-500, Feb. 2016.
[8] Z. Pan, Q. Guo, and H. Sun, "Feasible region method based integrated heat and electricity dispatch considering building thermal inertia," *Applied Energy*, vol. 192, pp. 395-407, Apr. 2017.
[9] Q. Zhou, Z. Tian, M. Shahidehpour *et al*., "Optimal consensus-based distributed control strategy for coordinated operation of networked microgrids," *IEEE Transactions on Power Systems*, vol. 35, no. 3, pp. 2452-2462, May 2020.
[10] Z. Ullah, G. Mokryani, and F. Campean, "Comprehensive review of VPPs planning, operation and scheduling considering the uncertainties related to renewable energy sources," *IET Energy System Integration*, vol. 1, no. 3, pp. 147-157, Sept. 2019.
[11] A. Baringo and L. Baringo, "A stochastic adaptive RO approach for the offering strategy of a virtual power plant", *IEEE Transactions on Power Systems*, vol. 32, no. 5, pp. 3492-3504, Sept. 2017.
[12] A. Baringo, L. Baringo, and J. M. Arroyo, "Day-ahead self scheduling of a virtual power plant in energy and reserve electricity markets under uncertainty," *IEEE Transactions on Power Systems*, vol. 34, no. 3, pp. 1881-1894, May 2019.
[13] F. L. Mueller, S. Woerner, and J. Lygeros, "Unlocking the potential of flexible energy resources to help balance the power grid," *IEEE Transactions on Smart Grid*, vol. 10, no. 5, pp. 5212-5222, Sept. 2019.
[14] H. Jin, Z. Li, H. Sun *et al*., "A robust aggregate model and the two-stage solution method to incorporate energy intensive enterprises in power system unit commitment," *Applied Energy*, vol. 206, pp. 1364-1378, Nov. 2017.
[15] H. Hao, B. M. Sanandaji, K. Poolla *et al.*, "Aggregate flexibility of thermostatically controlled loads," *IEEE Transactions on Power Systems*, vol. 30, no. 1, pp. 189-198, Jan. 2015.
[16] C. Chen, H. Sun, X. Shen *et al*., "Two-stage robust planning-operation co-optimization of energy hub considering precise energy storage economic model, " *Applied Energy*, vol. 252, p. 113372, Oct. 2019.
[17] R. Jiang, M. Zhang, G. Li *et al*., "Two-stage network constrained robust unit commitment problem," *European Journal of Operational Research*, vol. 234, no. 3, pp. 751-762, May 2014.
[18] B. Zeng and L. Zhao, "Solving two-stage robust optimization problems using a column-and-constraint generation method," *Operations Research Letters*, vol. 41, no. 5, pp. 457-461, Sept. 2013.
[19] Z. Li, J. Wang, H. Sun *et al*., "Robust estimation of reactive power for an active distribution system," *IEEE Transactions on Power Systems*, vol. 34, no. 5, pp. 3395-3407, Sept. 2019.
[20] T. Lipp and S. Boyd, "Variations and extension of the convex-concave procedure," *Optimization and Engineering*, vol. 17, pp. 263–287, Jun. 2016.
[21] H. Zhao, J. Chen, B. Wang *et al*., "A robust aggregate model for multi-energy virtual power plant in grid dispatch," *in Proceedings 2019 IEEE Sustainable Power and Energy Conference (iSPEC)*, Beijing, China, Nov. 2019, pp. 1631-1636.
[22] T. K. Wijaya, M. Vasirani, and K. Aberer, "When bias matters: An economic assessment of demand response baselines for residential customers," *IEEE Transactions on Smart Grid*, vol. 5, no. 4, pp. 1755–1763, Jul. 2014.
[23] Y. Zhang, W. Chen, R. Xu *et al*., "A cluster-based method for calculating baselines for residential loads," *IEEE Transactions on Smart Grid*, vol. 7, no. 5, pp. 2368-2377, Sept. 2016.
[24] R. Lahdelma and H. Hakonen, "An efficient linear programming algorithm for combined heat and power production," *European Journal of Operational Research*, vol. 148, no. 1, pp. 141-151, Jul. 2003.
[25] Gurobi 9.0.0 Homepage. [Online]. Available: https://www.gurobi.com/
[26] C. M. Correa-Posada and P. Sánchez-Martín, "Integrated power and natural gas model for energy adequacy in short-term operation," *IEEE Transactions on Power Systems*, vol. 30, no. 6, pp. 3347-3355, Nov. 2015.
[27] DIMS test system. (2020, Jan.). Test-data for active VPP. [Online]. Available: https://cloud.tsinghua.edu.cn/d/ba44885750e646118e79/
[28] North China Energy Regulatory Bureau. (2020, Jan.). Rules for operation of the North China Electric Power peak shaving ancillary service market. [Online]. Available: http://hbj. nea. gov. cn/adminContent/initViewContent.do?pk=e9bf9900-d3eb-4b72-88fb-49e829f891c8

Haotian Zhao received the B. S. degree from Xi'an Jiaotong University, Xi'an, China, in 2017. He is currently pursuing the Ph.D. degree in the Department of Electrical Engineering, Tsinghua University, Beijing, China. His research interests include the coordinated operation in integrated energy systems and virtual power plant.

Bin Wang received the B. S. and Ph. D. degrees in electrical engineering from Tsinghua University, Beijing, China, in 2005 and 2011, respectively. He is currently a Research Scientist with the Department of Electrical Engineering, Tsinghua University. His research interests include renewable energy optimal dispatch and control, automatic voltage control.

Xuanyuan Wang received the M. Sc. and Ph. D. degrees in electrical engineering from the University of Waterloo, Waterloo, Canada, and Tsinghua University, China, respectively. She is currently an Executive Director, General Manager of Jibei Power Exchange Center Co., Ltd., Beijing, China. Her research interests include power market regulation, electricity market, power system operations, power electronics and renewable energy.

Zhaoguang Pan received the B.S. and Ph.D. degrees from the Department of Electrical Engineering, Tsinghua University, Beijing, China, in 2013 and 2018, respectively. He is current a Post-doctor with Department of Electrical Engineering, Tsinghua University. His research interests include integrated energy systems, energy management and energy internet.

Hongbin Sun received the double B. S. degrees from Tsinghua University, Beijing, China, in 1992, the Ph.D. degree from Department of Electrical Engineering, Tsinghua University, in 1997. He is now Changjiang Scholar Chair Professor of Education Ministry of China, Tenured Full Professor of electrical engineering and the Director of Energy Management and Control Research Center in Tsinghua University. From Sept. 2007 to Sept. 2008, he was a Visiting Professor with School of Electrical Engineering and Computer Science (EECS) at the Washington State University, Pullman, USA. He is a Fellow of IEEE and IET. He is serving as the founding chair of IEEE PES Energy Internet Coordinating Committee (EICC). He served as the Founding Chair of IEEE Conference on Energy Internet and Energy System Integration in Nov. 2017. In recent 20 years, he led a research group in Tsinghua University to develop a commercial system-wide automatic voltage control system, which has been applied to more than 100 electrical power control centers in China as well as the control center of PJM interconnection, the largest regional power grid in USA. He won the China National Technology Innovation Award in 2008, the National Distinguished Teacher Award in China in 2009, and the National Science Fund for Distinguished Young Scholars of China in 2010. He awarded a First Prize of China National Technology Progress Award in 2018 for his pioneering achievement on "Automatic Voltage Control System (AVC) for complex power grids". He has published more than 500 peer-reviewed papers and 5 books. His Google Scholar citation is over 13000. He has been authorized over 100 Chinese Patents of Invention and 21 U.S. Patents. His research interests include energy management system, automatic voltage control, Energy Internet and energy system integration.

Zhen Liu received the M. Sc. degree in electrical engineering from Tsinghua University, Beijing, China. She is currently an Engineer in Jibei Power Exchange Center Co., Ltd., Beijing, China. Her research interests include virtual power plant, power electronics and flexible AC/DC transmission systems.

Qinglai Guo received the B.S. degree from the Department of Electrical Engineering, Tsinghua University, Beijing, China, in 2000. He received the Ph. D. degree from Tsinghua University in 2005. He is now an Associate Professor with the Department of Electrical Engineering, Tsinghua University. He is a member of CIGRE C2.13 Task Force on voltage/var support in system operations. His research interests include smart grids, cyber-physical systems and electrical power control center applications.